Wave-equation extended images via image-domain interferometry

Ivan Vasconcelos (ION Geophysical / GXT Imaging Solutions), Paul Sava (Colorado School of Mines), and Huub Douma (ION Geophysical / GXT Imaging Solutions)

SUMMARY

Using general two- and one-way representations for scattered wavefields, we analyze the nature of extended images obtained in wave-equation imaging. The presented formulation explicitly connects the wavefield correlations done in seismic imaging with the theory and practice of seismic interferometry. We show that extended images actually behave as locally scattered fields in the image domain. The wavefield behavior of two- and one-way extended images is illustrated using numerical examples. The general description of the extended images presented here and the derived insight that they actually are scattered fields in the image-domain, may prove to be useful in further development of imaging and inversion methods.

INTRODUCTION

Most wave-equation-based imaging methods rely on the cross-correlation of source and receiver wavefields to invoke the zero time-lag and zero space-lag imaging condition (e.g., Claerbout, 1985). This imaging condition has recently been extended by correlating wavefields with non-zero lags in the spatial coordinates also (Sava and Fomel, 2003). This allows, for example, studying the dependence of the image gathers on the velocity used in wave-equation-based imaging. Besides allowing for lags in the spatial coordinates when calculating the cross correlations, one can also allow for non-zero lags in the time variable (Sava and Fomel, 2006; Sava and Vasconcelos, 2009). We refer to the images obtained using non-zero lags in both the spatial and time variables as extended images.

In seismic interferometry the cross-correlation of wavefields received at two receivers allows the extraction of the response between these receivers as if one of them acted as a source (e.g., Curtis et al., 2006; Vasconcelos and Snieder, 2008). Representation theorems for the scattered field traveling from one point inside the medium to another can be found using scattering reciprocity relations (Vasconcelos and Snieder, 2008; Wapenaar et al., 2008). This theorem contains surface integrals just like in seismic interferomety. Since an image of a scatterer can be obtained by collapsing the recorded scattered wavefield onto the scatterer location, this formulation based on scattering representations can be used to interpret the imaging condition in the context of seismic interferometry (Vasconcelos, 2008): the image is the zero-time scattered-wave response generated by zero-offset pseudo-experiments in the image domain. Here we expand on this notion of "image-domain interferometry" and show that the representation theorems for the scattered field allow the extended images to be described as scattered wavefields which are "excited" and recorded in the image domain. We show this for both the one-way and two-way wave equation. For the sake of simplicty we assume throughout this work that the medium is acoustic, lossless, and that there is no scattering from density contrasts. We emphasize that these simplifications are purely formal and that the same treatment can be done for arbitrary wave or diffusion fields in lossy media.

SCATTERING REPRESENTATIONS

Two-way scattered fields

Let the scattered-field p_S be defined by the difference of a total perturbed field p and a reference field p_0, i.e., $p_S = p - p_0$. The frequency-domain scattered-wave $p_S(\mathbf{r}_B, \mathbf{r}_A, \omega)$, describing scattered waves propagating between any two points $\mathbf{r}_B$ and $\mathbf{r}_A$ inside a volume $\mathbb{V}$ bounded by a smooth surface $\partial\mathbb{V}$ (with outward-pointing normal $\mathbf{n}$), is given by (Vasconcelos, 2007; Vasconcelos and Snieder, 2008)

$$G_S(\mathbf{r}_B, \mathbf{r}_A, \omega) = \oint_{\partial\mathbb{V}} \frac{2F(\omega)}{\rho c} p_S(\mathbf{r}_A, \mathbf{r}, \omega) p_0^*(\mathbf{r}_B, \mathbf{r}, \omega)\, d^2\mathbf{r} + \int_{\mathbb{V}} \frac{F(\omega)}{i\omega\rho}\, p(\mathbf{r}_A, \mathbf{r}, \omega) V(\mathbf{r}) p_0^*(\mathbf{r}, \mathbf{r}_B, \omega)\, d^3\mathbf{r}\,, \quad (1)$$

where $G_S(\mathbf{r}_B, \mathbf{r}_A, \omega)$ is the Green function for the scattered field p_S recorded at location $\mathbf{r}_B$ due to a source at location $\mathbf{r}_A$, $F(\omega)$ is a waveform shaping filter that accounts for the power-spectrum of the source wavelet, ω is the harmonic frequency and ρ the spatially-varying density. The scattering potential $V = \omega^2(c^{-2} - c_0^{-2})$ describes the scattering properties of the medium in terms of the wavespeed contrast between the reference (c_0) and perturbed (c) media. For the sake of brevity, we used a far-field radiation condition (e.g., Vasconcelos and Snieder, 2008) in equation 1 to simplify the surface integral.

One-way scattered fields

Now we assume that a given pressure wavefield p (not necessarily impulsive) can be decomposed into an up-going component p^- and a down-going component p^+. These general up- and down-going fields are related through the reflectivity operator $R_0^+(\mathbf{r}_A, \mathbf{r}_B, \omega)$, which describes the up-going scattering response at $\mathbf{r}_A$ due to a downgoing impulsive reference field at $\mathbf{r}_B$. Therefore R_0^+ is the scattered response we are after when imaging in the context of one-way wavefield extrapolation.

An approximate scattered response can be found through cross-correlation of the down- and up-going wavefields (Wapenaar et al, 2008, equation 15), and is given by

$$R_0^+(\mathbf{r}_B, \mathbf{r}_A, \omega) \approx \int_{\partial\mathbb{V}_S} p^-(\mathbf{r}_B, \mathbf{r}_S, \omega) \{p^+(\mathbf{r}_A, \mathbf{r}_S, \omega)\}^*\, d^2\mathbf{r}_S\,; \quad (2)$$

where $\partial\mathbb{V}_S$ is a plane of integration (e.g. a horizontal plane at a given depth level). The subscript 0 in R_0^+ denotes that multiples related to reflectors above $\partial\mathbb{V}_S$ are not included.

Image-domain interferometry and wave-equation extended images

TWO- AND ONE-WAY EXTENDED IMAGES

Two-way imaging conditions

An image can be defined as the zero-lag scattered-wave response evaluated at every point $\mathbf{r}_I$ in the image space and at time equal zero (e.g., Claerbout, 1985). We can apply this imaging condition to the representation of the scattered field G_S in equation 1 to obtain the conventional image $I(\mathbf{r}_I) = G_S(\mathbf{r}_I,\mathbf{r}_I,t=0) = \int G_S(\mathbf{r}_I,\mathbf{r}_I,\omega)\,d\omega$. Doing this reveals that besides the conventional surface integral used in migration, there are also volume integrals that contribute to the image which are not used in migration (Vasconcelos, 2008). The extended images can be obtained in an analogous manner but allowing for a shift in both time and allowing the source and receiver locations to be different. Assuming a common image point $\mathbf{r}_I$, we write the source and receiver locations as $\mathbf{r}_I+\delta\mathbf{r}'$ and $\mathbf{r}_I+\delta\mathbf{r}'$ respectively. Using this in equation 1 then gives

$$\begin{aligned} I(\mathbf{r}_I,\delta\mathbf{r}',\tau) &= G_S(\mathbf{r}_I-\delta\mathbf{r}',\mathbf{r}_I+\delta\mathbf{r}',t=\tau) \\ &= \int\left(\oint_{\partial\mathbb{V}}\frac{2F(\omega)}{\rho c}\,p_S(\mathbf{r},\mathbf{r}_I+\delta\mathbf{r}',\omega)\,p_0^*(\mathbf{r},\mathbf{r}_I-\delta\mathbf{r}',\omega)d^2\mathbf{r}\right)e^{i\omega\tau}\,d\omega \\ &+\int\left(\int_{\mathbb{V}}\frac{F(\omega)}{i\omega\rho}\,p(\mathbf{r},\mathbf{r}_I+\delta\mathbf{r}',\omega)V(\mathbf{r})p_0^*(\mathbf{r},\mathbf{r}_I-\delta\mathbf{r}',\omega)\,d^3\mathbf{r}\right)e^{i\omega\tau}\,d\omega\,. \end{aligned} \tag{3}$$

Most current full-way migration schemes do not evaluate the volume integral above, and instead compute only a surface integral:

$$\begin{aligned} I(\mathbf{r}_I,\delta\mathbf{r}',\tau) &= G_S(\mathbf{r}_I-\delta\mathbf{r}',\mathbf{r}_I+\delta\mathbf{r}',t=\tau) \\ &= \int\left(\int_{\partial\mathbb{V}'}\frac{2F(\omega)}{\rho c}\,p_S(\mathbf{r},\mathbf{r}_I+\delta\mathbf{r}',\omega)\,p_0^*(\mathbf{r},\mathbf{r}_I-\delta\mathbf{r}',\omega)d^2\mathbf{r}\right)e^{i\omega\tau}\,d\omega; \end{aligned} \tag{4}$$

where $\partial\mathbb{V}'$ is a portion of the closed surface $\partial\mathbb{V}$. As opposed to conventional imaging, the image in equations 3 and 4 are not only functions of $\mathbf{r}_I$, but also of the space-lag vector $\delta\mathbf{r}'$ and of the time-lag parameter τ. These are the same space- and time-lags discussed by Sava and Vasconcelos (2009). While interferometry relies on observed fields p_0 and p_S (e.g., Vasconcelos, 2008), in wave-equation imaging these fields result from extrapolating (i.e., re-datuming) the fields recorded at the acquisition surface to the image point $\mathbf{r}_I$ (e.g., Claerbout, 1985; Sava and Vasconcelos, 2009). In imaging, $p_0(\mathbf{r},\mathbf{r}_I,\omega)$ are depth-extrapolated source wavefields, while $p_S(\mathbf{r},\mathbf{r}_I,\omega)$ are the image-domain scattered fields extrapolated from the recorded data. In conventional common-shot wave-equation migration, the cross-correlation of source and receiver fields followed by summation over shots at the surface corresponds to the evaluation of the surface integral in equation 1.

Equations 3 and 4 define common-image-point extended images, i.e., both source and receiver points in the image-wavefield $G_S(\mathbf{r}_I-\delta\mathbf{r}',\mathbf{r}_I+\delta\mathbf{r}',\tau)$ vary for a fixed $\mathbf{r}_I$. We analyze this particular type of extended image because it is a straightforward extension of the conventional common-image gathers used in wave-equation migration (e.g., Sava and Fomel, 2003; Sava and Vasconcelos, 2009). It is of course possible to conceive other types of extended images. For example, a common-source extended image would be given by $I(\mathbf{r}_I,\delta\mathbf{r}',\tau) = G_S(\mathbf{r}_I,\mathbf{r}_I+\delta\mathbf{r}',\tau)$.

One-way imaging conditions

Using equation 2 we can define one-way extended images in a manner analogous to the two-way definition in equation 4. In this case an extended image in the common-image domain is formed by calculating $R_0^+(\mathbf{r}_I-\delta\mathbf{r}',\mathbf{r}_I+\delta\mathbf{r}',t=\tau)$. Using equation 2 we then have

$$\begin{aligned} I(\mathbf{r}_I,\delta\mathbf{r}',\tau) &= R_0^+(\mathbf{r}_I-\delta\mathbf{r}',\mathbf{r}_I+\delta\mathbf{r}',t=\tau) \\ &= \int\left(\int_{\partial\mathbb{V}_S}p^-(\mathbf{r}_I-\delta\mathbf{r}',\mathbf{r}_S,\omega)\left\{p^+(\mathbf{r}_I+\delta\mathbf{r}',\mathbf{r}_S,\omega)\right\}^*d^2\mathbf{r}_S\right)e^{i\omega\tau}\,d\omega\,. \end{aligned} \tag{5}$$

Similar to the case of two-way extended images, equation 5 defines a common-image point image. A common-source extended image would be given by $I(\mathbf{r}_I,\delta\mathbf{r}',\tau) = R_0^+(\mathbf{r}_I,\mathbf{r}_I+\delta\mathbf{r}',t=\tau)$, and the most general extended image would be simply given by $R_0^+(\mathbf{r}_I,\mathbf{r},t=\tau)$.

INTERPRETING EXTENDED IMAGES

It follows from equations 4 and 5 that extended images can be interpreted as scattered wavefiels with sources (at $\mathbf{r}_I-\delta\mathbf{r}'$) and receivers (at $\mathbf{r}_I+\delta\mathbf{r}'$) in the image domain, and τ as the running time variable. We illustrate this using examples for both two-way and one-way extended images.

Two-way extended images

Figure 1 shows an example of the asymptotic phase behavior of the extended image in equation 4. In Figure 1a, when the image point is coincident with the scatterer location (i.e., $\mathbf{r}_I=\mathbf{x}_S$), the non-zero value of the extended image at the origin yields the traditional image. Away from the origin, Figure 1a depicts the traveltimes of transmitted scattered waves excited at $\mathbf{r}_I-\delta\mathbf{r}'$ and recorded at $\mathbf{r}_I+\delta\mathbf{r}'$. When the image point is not coincident with the scatterer location (i.e., $\mathbf{r}_I\neq\mathbf{x}_S$, Figure 1b), the extended image vanishes at the origin, because any scattered wave will have a finite traveltime for the experiment where both pseudo-source and receiver lie at $\mathbf{x}_S$. For points that are not at the origin of Figure 1b, the depicted traveltime can correspond to either a back- or a forward-scattered wave, depending on the position of the scatterer at $\mathbf{x}_S$ relative to the points $\mathbf{r}_I\pm\delta\mathbf{r}'$.

Note that the asymptotic behavior of two-way extended images illustrated in Figures 1a-b is inferred directly from the traveltimes of scattered waves, i.e., in terms of $G_S(\mathbf{r}_I-\delta\mathbf{r}',\mathbf{r}_I+\delta\mathbf{r}',t=\tau)$ (the left-hand side of equation 3). Therefore, there could be important practical differences between the two-way extended images as depicted by Figures 1a-b with those actually computed via standard two-way migration methods (equation 4). Further analysis and numerical testing to elucidate the differences between equations 3 and 4 are the subject of ongoing research.

One-way extended images

Analogous to their two-way counterparts, one-way extended images also behave as wavefields, described by the reflectivity operator R_0^+ (equation 2). In Figure 2a, we show $R_0^+(\mathbf{r}_I, \mathbf{r}, t = 0)$ at a given image depth in explicit matrix form. The conventional zero-lag image lies in the principal diagonal of R_0^+ (highlighted with black dots), i.e., where the pseudo-source and pseudo-receiver image points are the same (i.e., $\mathbf{r}_I = \mathbf{r}$). Extended images are obtained by including off-diagonal elements of R_0^+. Note that, for depth-domain one way extrapolation, the off-diagonal elements in Figure 2a correspond to horizontal lags only as the source and receiver locations $\mathbf{r}_I - \delta\mathbf{r}'$ and $\mathbf{r}_I + \delta\mathbf{r}'$ need to coincide with source and receiver positions already contained in the matrix. The matrix columns (in blue) yield image gathers of the common-source type, while the data in the rows (in green) result in common-receiver image-gathers. The more traditional common-image-point gathers, $I(\mathbf{r}_I, \delta\mathbf{r}', \tau = 0)$ are given by the diagonal elements highlighted in red.

Ideally, the one-way extended images should be estimated through a multidimensional deconvolution process at every depth (Wapenaar et al., 2008, equation 11). Here, however, we focus on the behavior of the approximate correlation-based extended images, described by equation 5. Figures 1c and 1d show the predicted phase of one-way extended images in the single scatterer case. One-way operators have decreasing accuracy towards horizontal progagation directions. This causes the one-way responses R_0^+ in Figures 1c and 1d to essentially be limited-aperture versions of the two-way images in Figures 1a and 1b.

To further elucidate the behavior of the extended image $I(\mathbf{r}_I, \delta\mathbf{r}', \tau)$, we illustrate the stationary contributions to the integrand in Figures 2b and 2c. For point diffractors (Figure 2), there are many stationary sources (e.g., both $\mathbf{r}'_S$ and $\mathbf{r}''_S$). For any pair $(\mathbf{r}_I - \delta\mathbf{r}', \mathbf{r}_I + \delta\mathbf{r}')$ lying on a stationary path (solid lines in Figure 2b), there is a contribution to the extended image at $\tau = 0$ because the up-going field at $\mathbf{r}_I - \delta\mathbf{r}'$ has the same traveltime as the down-going wave at $\mathbf{r}_I + \delta\mathbf{r}'$. Thus, for varying $\delta\mathbf{r}'$, every stationary source yields a non-zero contribution along a straight line in the $[\delta\mathbf{r}'_1, \delta\mathbf{r}'_2]$-plane (here the 2D vertical plane that contains the vectors $\mathbf{r}_I - \delta\mathbf{r}'$ and $\mathbf{r}_I + \delta\mathbf{r}'$) that coincides with the stationary path. In the single-scatterer case (Figure 2b), the superposition of many such straight lines associated to all available stationary points effectively results in a band-limited point in an extended image at $\mathbf{r}_I = \mathbf{x}_S$ (see also Figure 1c). This scenario changes if the waves are scattered by a horizontal interface, as in Figure 2c. In that case, the only stationary source contribution is at $\mathbf{r}'_S$ which yields a stationary path along a straight vertical line (Figure 2c). So, unlike the point-scatterer case, the extended image corresponding to Figure 2c will depict a straight line in the $[\delta\mathbf{r}'_1, \delta\mathbf{r}'_2]$-plane that is always perpendicular to the interface: a vertical line in this case.

In Figure 3, we show a numerical example of the one-way extended images. The model contains point scatterers as well as horizontal and dipping interfaces (Figure 3a). We show the extended images (Figures 3b through 3d) at three different locations in the conventional image (red points in Figure 3a). At the point diffractor (Figure 3a) and using the correct wavespeed model, the one-way extended image response is a band-limited point at the origin. This agrees with our analysis of the behavior of one-way extended images shown in Figures 2b and 1c. Also, as explained using the cartoon in Figure 2c, the one-way extended images at the interfaces (Figures 3c and 3d) focus around $\tau = 0$ and along straight lines that are perpendicular to the local interface dip.

DISCUSSION

By describing extended images as local wavefields, we offer a generalized formulation to perform image-domain analyses that can have several potential advantages. Because our formulation does not rely on single scattering approximations, it could allow for the inclusion of effects such as multiple scattering and transmission, e.g., for potential migration of free-surface or internal multiples. In the case of two-way imaging (e.g., reverse-time migration) of multiple scattered waves (e.g. multiples, "prismatic" arrivals), we expect that the volume integral terms that are currently ignored will be useful in dealing with including sharp boundaries in the background models. In this context, extended images may help in formally describing and treating migration/imaging features such as, for instance, the commonly observed low-spatial-frequency artifacts in reverse-time migration.

In a companion paper, Sava and Vasconcelos (2009) demonstrate that extended images may provide additional sensitivity to the background migration wavespeed model. Thus, we believe that the formulation we present here possibly allows for further development of image-domain inversion methods for reflectivity and/or wavespeed models that take advantage of the structure of fully extended images.

CONCLUSION

We have shown that one-way as well as two-way wave-equation-based extended images are equivalent with locally scattered wavefields in the image domain, and have presented numerical examples to illustrate and explain the behavior of these images for the canonical examples of point-scatterers and planar reflectors. In addition we have made clear the close connection between the extended images and seismic interferometry. The general description of the extended images and their interpretation as locally scattered wavefields in the image domain may prove to be useful in further development of imaging and inversion algorithms.

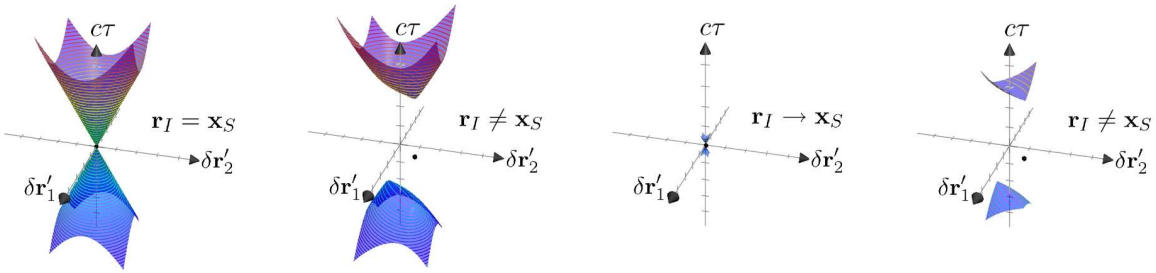

(a) **(b)** **(c)** **(d)**

Figure 1: Asymptotic phase behavior of common-image-point extended images (at $\mathbf{r}_I$) for the case of a single point scatterer at $\mathbf{x}_S$, embedded in a 2-D homogeneous space. Panels (a) and (b) represent the extended images of in two-way imaging (equation 4), while (c) and (b) are the their one-way counterparts. These responses correspond to a medium with constant background wavespeed c. Note that the responses are depicted for normalized traveltimes $c\tau$. In all plots, the black dot denotes the position of the scatterer (i.e. $\mathbf{x}_S$) with respect to the image point (i.e., $\mathbf{r}_I$ is at the origin).

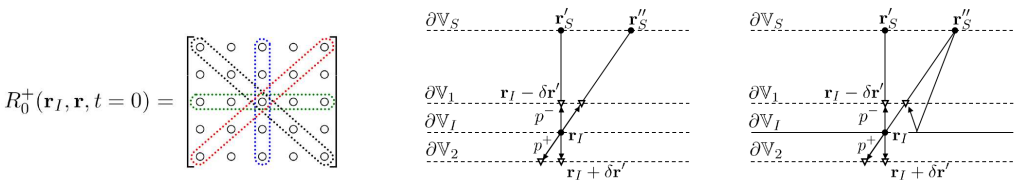

(a) **(b)** **(c)**

Figure 2: Behavior of one-way extended images. Panel (a) shows the structure of the zero-lag reflectivity operator R_0^+ in matrix form, at a given image level (e.g., for a fixed depth and with variable horizontal coordinates). Panels (b) and (c) relate to the behavior of one-way common-image-point extended images for the cases where scattering comes from a single scatterer, in (b), and from a plane horizontal interface, in (c). In both (b) and (c), the black dot denotes the image point $\mathbf{r}_I$, and triangles represent image-lag points $\mathbf{r}_I \pm \Delta\mathbf{r}$. The points $\mathbf{r}'_S$ and $\mathbf{r}''_S$ are two arbitrary source points from the integrand of equation 5.

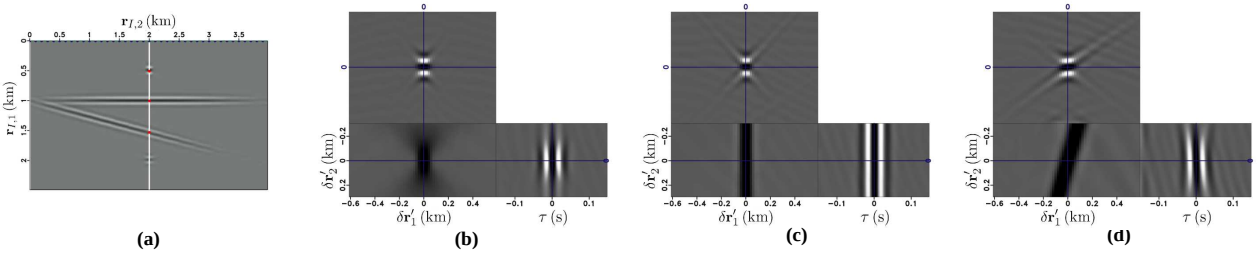

(a) **(b)** **(c)** **(d)**

Figure 3: Numerical example of one-way extended images. Panel (a) is the conventional seismic image, where the red dots indicate the locations where extended images are evaluated. The corresponding extended images are shown in (b) at the point scatterer, in (c) at the horizontal reflector, and in (d) for the dipping reflector.